ELSEVIER

Polymer 41 (2000) 8941–8951

polymer

www.elsevier.nl/locate/polymer

A calibration of complex heat capacity obtained by temperature-modulated DSC in the melting region of polymer crystals ☆

A. Toda*, T. Arita, C. Tomita, M. Hikosaka

Faculty of Integrated Arts and Sciences, Hiroshima University, 1-7-1 Kagamiyama, Higashi-Hiroshima 739-8521, Japan

Received 24 September 1999; received in revised form 25 January 2000; accepted 4 February 2000

Abstract

Complex heat capacity obtained in melting region of polymer crystals by temperature-modulated differential scanning calorimetry of heat flux type has been calibrated with a method based on a model proposed by Hatta. The calibration method corrects for the effect of thermal conductivity of the DSC apparatus on the magnitude and phase angle of the heat capacity. The validity of the correction has been confirmed by examining the reversible melting and crystallization of indium under quasi-isothermal conditions. For the irreversible melting of polymer crystals analyzed with an additional underlying heating rate, the calibrated heat capacity becomes a complex quantity with a frequency dependence roughly approximated by Debye's type, the characteristic time of which depends on the underlying heating rate. This behavior qualitatively agrees with the previous results obtained by the calibration of baseline-subtraction from the phase angle. The applicability of the "baseline-subtraction" has also been discussed.

Keywords: T-MDSC; Calibration; Complex heat capacity; Phase angle; Melting of polymer crystals

1. Introduction

We have recently proposed an analysis method of melting and crystallization of polymer crystals with temperature-modulated differential scanning calorimetry (T-MDSC) [1–8]. In T-MDSC one applies a temperature modulation to a conventional DSC run and determines an apparent heat capacity from the modulation components of temperature and the heat flow response [9–11].

In the melting region of polymer crystals, the apparent heat capacity becomes a complex quantity. It has been pointed out that the thermal conductivity and the heat capacity of the instrument have an additional contribution to magnitude and phase angle of the complex heat capacity [12–15]. It is also known that the heat capacity of the sample influences these contributions and makes the calibration more complicated. Therefore, the important point in any analysis is the appropriate calibration of the magnitude and phase angle, as has been argued frequently [16–21]. Considering these effects, Hatta [22] has presented a calibration method for the heat capacity obtained with T-MDSC of the heat flux type. The method is unique in utilizing a master curve of calibration as a function of phase angle and is free from undetermined parameters when a real heat capacity is concerned. In the present paper, we extend this method to the complex heat capacity obtained in the melting region of polymer crystals. The analysis provides valuable information about the melting kinetics, for which microscopy is not practical because of the complexity of the process.

In the following, we first examine the heat capacity of aluminum as a typical example of a real heat capacity and discuss the dependence of the raw data on modulation frequency and on sample heat capacity. Based on Hatta's model, we examine the calibration of magnitude and phase angle which should be zero for a real heat capacity. With the knowledge of instrument's coefficients, a calibration method of complex heat capacity is presented for T-MDSC of the heat flux type. We test the applicability of the method experimentally for reversible melting and crystallization of indium under quasi-isothermal conditions and the irreversible melting of polymer crystals when using an underlying heating rate.

2. Experimental

A DSC 2920 Module controlled with a Thermal Analyst

☆ Presented in part at the Symposium on Semicrystalline Polymers in Memory of Andrew Keller held in Fall Meeting of American Chemical Society, New Orleans, Louisiana, 23–26 August 1999.

* Corresponding author. Tel.: +81-824-24-6558, fax: +81-824-24-0757.

E-mail address: atoda@hiroshima-u.ac.jp (A. Toda).

0032-3861/00/$ - see front matter
PII: S0032-3861(00)00237-8

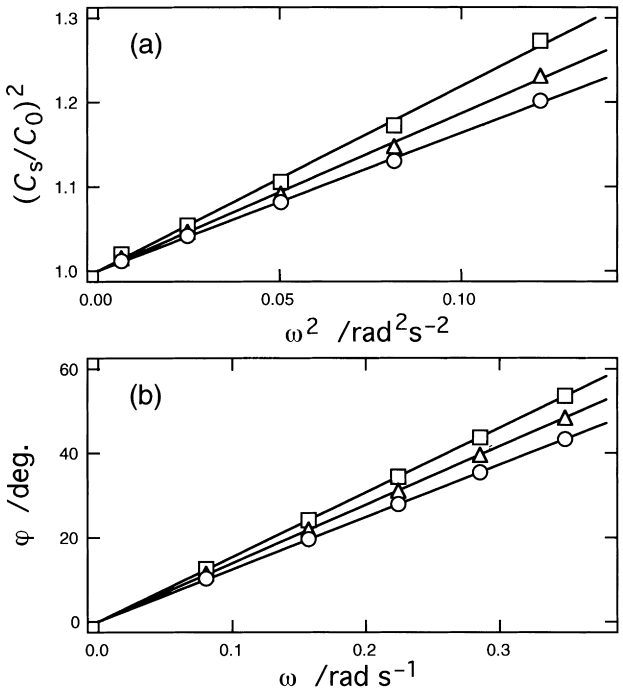

Fig. 1. Plots of: (a) $(C_s/C_0)^2$ against ω^2; and (b) φ against ω for the quasi-isothermal measurements of aluminum at −12°C. The modulation periods were 18, 22, 28, 40 and 78 s. The heat capacity of the aluminum sample and pan was 34.0 (○), 48.9 (△) and 62.2 mJ K^{-1} (□). The purge gas was helium. The modulation amplitude was 0.2 K.

2200 (TA Instruments) was used for all measurements. Nitrogen or helium gas with a flow rate of 40 ml min^{-1} was purged through the cell. The reference pan was removed in the experiments to analyze the data by Hatta's model, described below.

For the examination of the heat capacity of aluminum, a disk-shaped thin sheet has been prepared (4.70 mg in weight, 95 μm thick). The number of sheets was changed from 0 (sample pan only) to 14 pieces, to examine the dependence of calibration on the sample heat capacity. The polymer samples were polyethylene (NIST SRM1475 of $M_w = 5.2 \times 10^4$ and $M_w/M_n = 2.9$) and poly(caprolactam) (nylon 6, Scientific Polymer Products, Inc.),

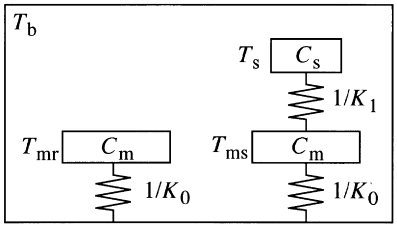

Fig. 2. Schematic representation of the models describing a DSC of heat flux type employed in Hatta's model of T-MDSC without a reference pan [22]. In the figures, T_b, T_{mr} and T_{ms} represent the temperatures of the block and the base plate at reference and sample sides, respectively. The Newton's law constants of heat transfer between the block and the base plate and between the base plate and the sample are K_0 and K_1, respectively. The heat capacity of the base plate is represented as C_m.

which were also disk-shaped thin films. The thickness of the polymer films was less than 100 μm for most experiments, and thicker films were prepared for the purpose of the examination of the effect of sample thickness.

For the calibration of the complex heat capacity, it is essential to have a fixed condition of thermal conductivity between the bottom of the sample pan and the base plate. In order to reduce the undesirable change for different sample pans, the size of the disk-shaped sheets of sample was chosen to fit the interior of the sample pan so that the crimping process causes minimum deformation of the bottom of the pan.

The examined modulation period was in the range of 10–100 s. Since smaller amplitude enables shorter modulation period, special attention to the modulation amplitude was required for the period below 30 s. For the quasi-isothermal experiment with aluminum, the modulation amplitude was 0.2 K. For the quasi-isothermal measurements of the reversible melting and crystallization of indium, the mean temperature was kept for 30 min at each temperature with the modulation amplitude of 0.02 K, followed by the increment of at least 0.04 K to repeat the measurement until the completion of melting. The modulation amplitude, $\tilde{T}_s$, for the irreversible melting of polymer crystals with an additional linear heating was adjusted for the condition of heating only, $(dT_s/dt > 0)$, and the maximum amplitude was set at 0.2 K. The heating-only condition with the underlying heating rate, β, and the angular frequency of modulation, ω, is expressed as $(\tilde{T}_s < \beta/\omega)$. For example, the amplitude was 0.02 K for the heating rate of 0.8 K min^{-1} with the period of 10 s. Temperature control in those experiments was checked by plotting Lissajous diagrams of the modulated heat flow versus temperature.

3. Calibration method

First, we define the heat capacity obtained by a T-MDSC. From the modulation components of sample temperature, $T_s = \bar{T}_s + \mathrm{Re}[\tilde{T}_s\, e^{i(\omega t+\epsilon)}]$, and of heat flow, $\dot{Q} = \bar{\dot{Q}} + \mathrm{Re}[\tilde{\dot{Q}}\, e^{i(\omega t+\delta)}]$, a heat capacity, $C_0\, e^{-i\varphi} \equiv C_0' - i\, C_0''$, is defined as,

$$C_0\, e^{-i\varphi} = \frac{\tilde{\dot{Q}}}{\omega\, \tilde{T}_s}\, e^{-i(\epsilon-\delta-(\pi/2))}. \tag{1}$$

Fig. 1 shows the frequency dependence of the calibration coefficient of magnitude, C_s/C_0, and of the phase angle, φ, for a true heat capacity, C_s, of aluminum. It is clearly seen that the values obtained are strongly dependent on frequency, while the true heat capacity must be a constant without imaginary part ($\varphi = 0$). The frequency dependence can be expressed as,

$$\left(\frac{C_s}{C_0}\right)^2 = 1 + A\omega^2, \tag{2}$$

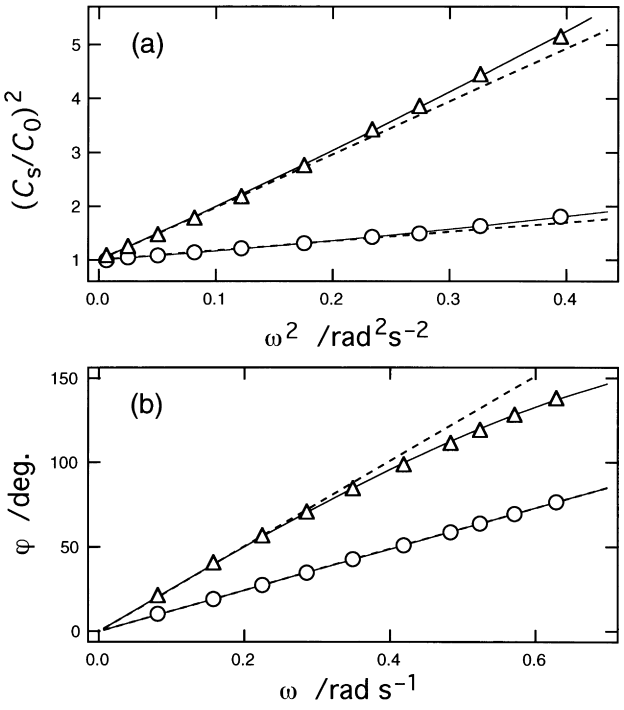

Fig. 3. Plots of: (a) $(C_s/C_0)^2$ against ω^2; and (b) φ against ω for the quasi-isothermal measurements of aluminum at −12°C with helium (○) and nitrogen (△) purge gases in a wide frequency range. The broken and full lines represent the fitting to Eqs. (2) and (3) and Eqs. (7) and (8), respectively. The modulation periods were 10, 11, 12, 13, 15, 18, 22, 28, 40 and 78 s. The heat capacity of aluminum sample and pan was 34.0 mJ K^{-1}. The modulation amplitude was 0.2 K.

$$\varphi = B\omega, \tag{3}$$

where A and B are constants. In the experimental results shown in Fig. 1, the coefficients, A and B, show a systematic dependence on the sample heat capacity, C_s. This is due to the fact that a DSC of the heat flux type, such as the DSC 2920 employed in the present experiments, does not directly measure the temperature of sample. Therefore, we must consider the thermal conductance between sample pan and base plate. Hatta's model [22] handles this effect, as shown in Fig. 2.

From Hatta's model, the following relationship is obtained for the raw data, $C_0\,e^{-i\varphi}$, and the true heat capacity, C_s, of sample and pan [22],

$$\frac{C_s}{C_0\,e^{-i\varphi}} = \left(1 + i\omega\frac{C_m}{K_0}\right)\left(1 + i\omega\frac{C_s}{K_1}\right), \tag{4}$$

and hence the frequency dependence has the coefficient, (C_s/K_1), depending on the sample heat capacity. When the conditions of

$$\frac{C_m}{K_0}\omega \ll 1 \text{ and } \frac{C_s}{K_1}\omega \ll 1$$

are satisfied, we obtain the following expansions of the calibration coefficients of magnitude, (C_s/C_0), and the phase angle, φ,

$$\left(\frac{C_s}{C_0}\right)^2 = 1 + \omega^2\left[\left(\frac{C_m}{K_0}\right)^2 + \left(\frac{C_s}{K_1}\right)^2\right] + \omega^4\left(\frac{C_m}{K_0}\frac{C_s}{K_1}\right)^2, \tag{5}$$

$$\varphi = \omega\left(\frac{C_m}{K_0} + \frac{C_s}{K_1}\right) - \frac{1}{3}\omega^3\left[\left(\frac{C_m}{K_0}\right)^3 + \left(\frac{C_s}{K_1}\right)^3\right] + \cdots \tag{6}$$

The expansion about frequency will be justified by the experimental results shown in Fig. 1. The detailed examination in a wider frequency region is shown in Fig. 3; because of lower thermal conductivity (smaller K_1) with nitrogen, the higher terms are actually required for the fitting of the data with nitrogen purge gas, namely,

$$\left(\frac{C_s}{C_0}\right)^2 = 1 + A\omega^2 + C\omega^4, \tag{7}$$

$$\varphi = B\omega - D\omega^3. \tag{8}$$

By examining the frequency dependence with different sample masses, we obtained the dependence of the coefficients A and B on the sample heat capacity. The results are

$$A = A_0 + A_1C_s^2, \tag{9}$$

$$B = B_0 + B_1C_s, \tag{10}$$

with constants, A_0, A_1, B_0 and B_1, as shown in Fig. 4 for nitrogen and helium purge gases. Therefore, the coefficients, A and B, show the dependence on the sample heat capacity, as expressed in Eqs. (5) and (6). The larger slopes, A_1 and B_1, for nitrogen purge gas must be due to the lower thermal conductivity of nitrogen, which decreases the heat-transfer coefficient, K_1, between the bottom of the sample pan and the base plate.

The slopes, A_1 and B_1, follow the relationship,

$$A_1 = B_1^2\left(= \frac{1}{K_1^2}\right),$$

expected from Eqs. (5) and (6), while another relation,

$$A_0 = B_0^2\left(= \left(\frac{C_m}{K_0}\right)^2\right),$$

does not hold. In order to incorporate the discrepancy, we must introduce an asymmetry in C_m and K_0 for the sample and reference sides. Then, Eqs. (4)–(6) are modified as follows,

$$\frac{C_s}{C_0\,e^{-i\varphi}} = (1 + i\omega\tau_m)\left(1 + i\omega\frac{C_s}{K_1}\right)(\kappa - i\omega\delta_m)^{-1}, \tag{11}$$

$$\left(\kappa\frac{C_s}{C_0}\right)^2 \cong 1 + \omega^2\left[\tau_m^2 - \left(\frac{\delta_m}{\kappa}\right)^2 + \left(\frac{C_s}{K_1}\right)^2\right], \tag{12}$$

$$\varphi \cong \omega\left(\tau_m + \frac{\delta_m}{\kappa} + \frac{C_s}{K_1}\right), \tag{13}$$

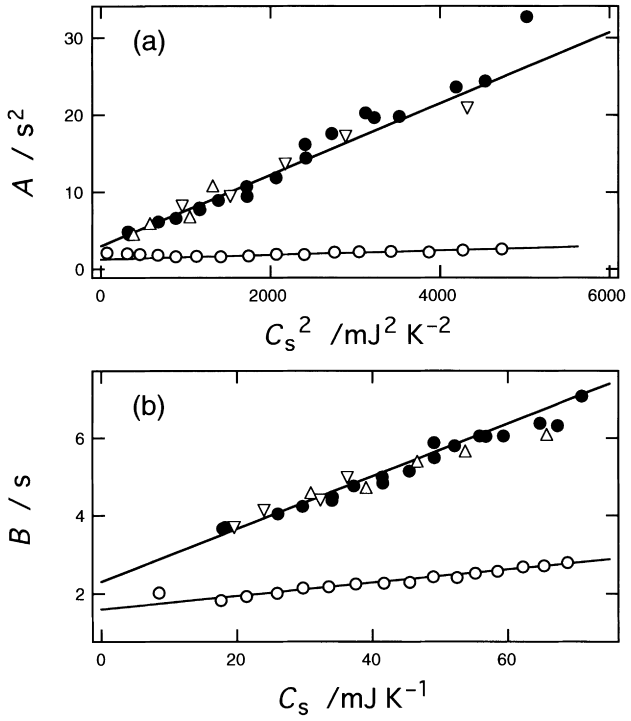

Fig. 4. The coefficients, A and B, of Eqs. (2) and (3) or of Eqs. (7) and (8) plotted against C_s^2 and C_s, respectively, for the purge gases of helium (○) and nitrogen (●). The coefficients were determined from the slopes of the plots such as are shown in Figs. 1 and 3. The symbols △ and ▽ are the results of polyethylene and aluminum sheets on thin polyethylene film, respectively.

where

$$\tau_m \equiv \frac{C'_m}{K'_0} \quad \text{and} \quad \kappa \equiv 1 - \delta_m \frac{K_1}{C_s}.$$

The asymmetry is represented by

$$\delta_m \equiv \left(\frac{K_0}{K_1}\right)\left(\frac{C'_m}{K'_0} - \frac{C_m}{K_0}\right)$$

with (C_m/K_0) and (C'_m/K'_0) designated for the sample and reference sides, respectively. On fitting the expressions of Eqs. (12) and (13) to the experimental data, we could set $\kappa \simeq 1$ except for the case of small C_s with helium purge gas. For C_s smaller than 20 mJ K^{-1}, the plot of the data with helium purge gas in Fig. 4 shows an upward shift, which must be due to the dependence of κ on C_s. The dependence can be appreciable only for very small amount of sample because the heat capacity of the sample pan is as large as 19 mJ K^{-1}.

Based on the above expressions with $\kappa = 1$, the coefficients, τ_m, δ_m and $(1/K_1)$, has been determined experimentally from the dependence on frequency and sample heat capacity. To see the effect of temperature, the dependence has been examined at several temperatures, as shown in Fig. 5. The coefficients are weakly dependent on temperature, probably due to better thermal conductivity at higher

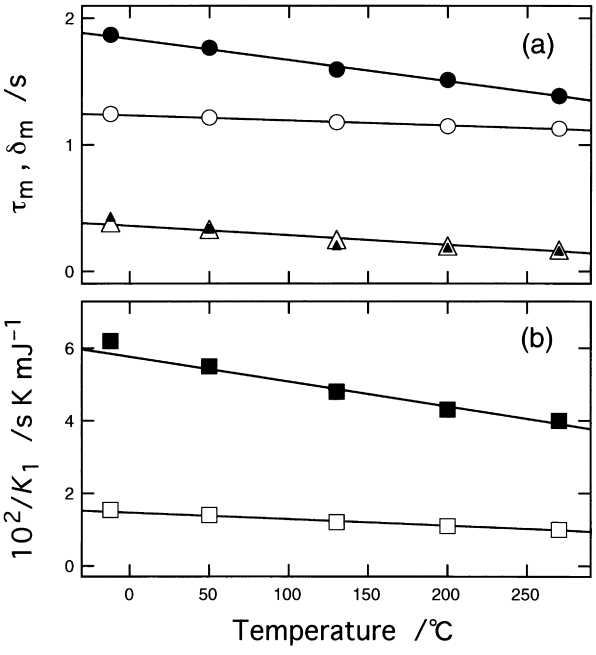

Fig. 5. Temperature dependence of the coefficients, τ_m (○, ●), δ_m (△, ▲) and $(1/K_1)$ (□, ■) for helium and nitrogen purge gases, respectively, determined from the slopes such as are shown in Fig. 4 by Eqs. (12) and (13).

temperatures. The fitting lines in Fig. 5 for the helium purge gas are τ_m/s $= 1.2 - 4.0 \times 10^{-4}\ T_s$/°C, δ_m/s $= 0.36 - 7.4 \times 10^{-4}\ T_s$/°C and $10^2\ K_1^{-1}$/s K mJ$^{-1} = 1.5 - 1.8 \times 10^{-3}\ T_s$/°C and for nitrogen purge gas τ_m/s $= 1.8 - 1.7 \times 10^{-3}\ T_s$/°C, δ_m/s $= 0.34 - 7.5 \times 10^{-4}\ T_s$/°C and $10^2\ K_1^{-1}$/s K mJ$^{-1} = 5.8 - 6.9 \times 10^{-3}\ T_s$/°C.

We have also examined the flow rate of purge gas in the range of 30–50 ml min^{-1}. The change in the flow rate had only a minor effect on the coefficients; the change was less than 1%. It is further noted that the thermal contacts between aluminum sheet and sample pan and between polymer film and sample pan should be different. The difference can affect the calibration coefficients if the thermal contact between polymer film and sample pan is as worse as the contact between the base plate and sample pan. The effect has been examined with polyethylene samples of different thickness and with the insertion of thin polyethylene film (~30 μm) at the bottom of aluminum sheets. The obtained results in Fig. 4 were in good agreement with the above results of aluminum sheets, and hence the effect could be neglected when polymer film was analyzed. Based on those results, the coefficients, τ_m, δ_m and $(1/K_1)$, will be certainly applied to the experiments of polymer samples. The coefficients however will not be identical for different instruments and will be subject to variation after the elapse of time, as is the case for the cell constant of conventional DSC. Therefore, periodical examination of the coefficients with each instrument will be recommended.

Among the terms in Eq. (11), (C_s/K_1) is the only indeterminate parameter and τ_m and δ_m the instrument coefficients. Therefore, for a given modulation period with a choice of

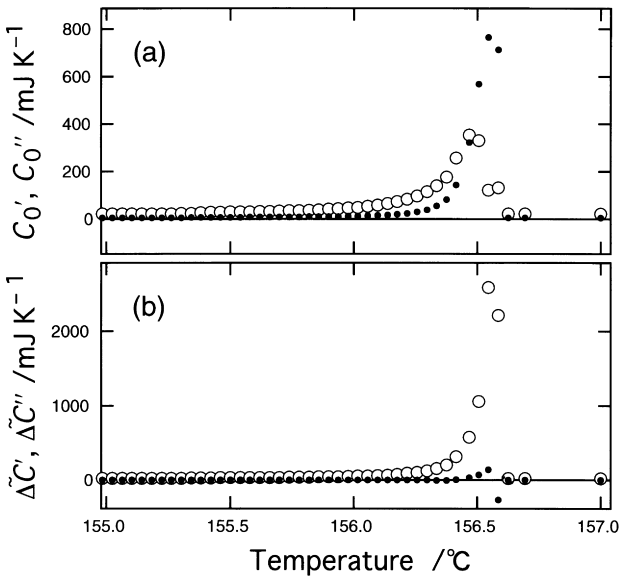

Fig. 6. The real (○) and imaginary (●) parts of: (a) the raw data; and (b) the calibrated heat capacity for the quasi-isothermal measurements in the melting region of indium of 11.97 mg. The calibration is based on Eq. (15). The modulation period was 60 s. The purge gas was helium.

purge gas and temperature, Eqs. (12) and (13) suggest that the calibration coefficient, (C_s/C_0), and the phase angle, φ, are related by the parameter, (C_s/K_1) and hence the plot of (C_s/C_0), against φ is expected to be on a master curve. In Hatta's calibration method [22], the master curve prepared with known samples is utilized to obtain the calibration coefficient of an unknown sample from the phase angle. Therefore, the method does not require the value of the indeterminate parameter, (C_s/K_1).

When the heat capacity of the sample is a complex quantity, the method is not applicable because of the imaginary part of complex heat capacity. This is the case when we examine the melting region of polymer crystals. For a complex heat capacity, $\widetilde{\Delta C}\,\mathrm{e}^{-\mathrm{i}\alpha} \equiv \widetilde{\Delta C}' - \mathrm{i}\,\widetilde{\Delta C}''$, the relation represented by Eq. (11) becomes

$$\frac{\widetilde{\Delta C}\,\mathrm{e}^{-\mathrm{i}\alpha}}{C_0\,\mathrm{e}^{-\mathrm{i}\varphi}} \cong (1+\mathrm{i}\omega\tau_\mathrm{m})\left(1+\mathrm{i}\omega\frac{\widetilde{\Delta C}\,\mathrm{e}^{-\mathrm{i}\alpha}}{K_1}\right)(1-\mathrm{i}\omega\,\delta_\mathrm{m})^{-1}. \tag{14}$$

In order to calibrate the heat capacity, the relation is rearranged as,

$$\frac{\mathrm{e}^{\mathrm{i}\alpha}}{\widetilde{\Delta C}} \cong \frac{\mathrm{e}^{\mathrm{i}\varphi}}{C_0}(1-\mathrm{i}\omega\delta_\mathrm{m})(1+\mathrm{i}\omega\tau_\mathrm{m})^{-1} - \mathrm{i}\frac{\omega}{K_1}. \tag{15}$$

where the coefficients, δ_m, τ_m and $(1/K_1)$, have been determined for the known samples of aluminum, as described above. Therefore, if we can assume that the change in the heat-transfer coefficient, (ω/K_1), is negligible among different sample pans, we will be able to obtain the magnitude, $\widetilde{\Delta C}$, and the phase angle, α, of the complex heat capacity from the raw data of C_0 and φ by Eq. (15). This assumption will be justified by the fact that the experimental results obtained with different samples shown in Fig. 4 are in accordance with the prediction of the modeling. From the degree of scatter of the data points in Fig. 4, the variation in $(1/K_1)$, for different sample pans is expected to be less than 10%.

4. Application 1

We first examine the reversible melting and crystallization of indium under quasi-isothermal condition [23]. The process undergoes an oscillatory movement of the interface, unless melting is complete. Therefore, we expect a steady state response of the reversible processes to the temperature modulation. Since the oscillatory movement will be able to follow the temperature modulation without delay for the period T-MDSC can apply, i.e. 10–100 s, the heat flow produced by the reversible processes will be indistinguishable from the heat flow due to the true heat capacity [24]. In such a case, the apparent heat capacity in the transition region will also be a real quantity without the imaginary part, and hence the calibration with Eq. (11) will be applicable. The reversible processes give a quite large apparent heat capacity, which enables us to examine the applicability of the calibration method for the large value of apparent heat capacity.

We have experimentally examined the behaviors in indium by applying a small modulation of 0.02 K under quasi-isothermal condition, followed by an increment of temperature (≥0.04 K) repeated until completion of melting (Fig. 6). In Fig. 6, the melting region extends over about 0.2 K. The breadth of the melting region will be mainly due to temperature gradient in the sample of relatively large quantity of 11.97 mg; the temperature gradient in the sample enables the oscillatory movement of the interface to have a steady state response to the temperature modulation. It should also be noted that the possibility of purity problem could not be excluded, while purity does not cause any essential problem in this analysis.

We first confirmed the reversible response of melting and crystallization without delay by examining the higher harmonics in the modulated heat flow. It was confirmed that there was no meaningful difference in the ratio of the second harmonic to the first harmonic in the melting region and out of the region and in the ratio of modulated heat flow and that of sample temperature; the ratio was not exactly zero (less than 1%) because of the slight fluctuation of sample temperature from exact temperature control. These evidences directly suggest the linear response of the oscillatory movement of the interface.

For the melting region, while the raw data in Fig. 6a have a quite large peak in the imaginary parts of the heat capacity, it is confirmed that the calibrated heat capacity in Fig. 6b has a very small imaginary part. Fig. 7 shows the frequency dependence of the heat capacity at its peak temperature. It

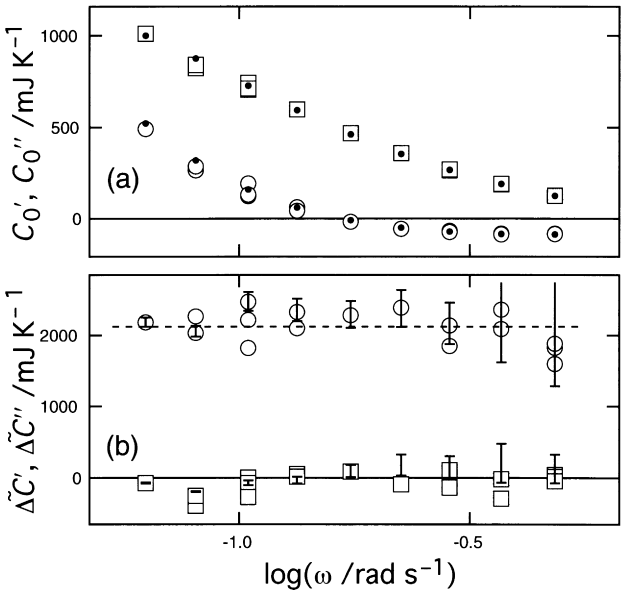

Fig. 7. Frequency dependence of the real (○) and imaginary (□) parts of the apparent heat capacity taken at the peak temperature in the plot such as shown in Fig. 6. The raw data and the calibrated results are shown in (a) and (b), respectively. The symbol, ●, in (a) represents the values calculated from the mean value of the calibrated real part in (b) (broken line) using Eq. (11). The error bars in (b) are calculated on the assumption of 1% error in the raw data.

is seen that the major part of the calibrated heat capacity is in the real part and shows no systematic dependence on frequency. Such results mean that the reversible melting and crystallization of indium follow the temperature modulation without delay, as expected. Fig. 7a further shows that the raw data is well reproduced by the values calculated from the mean value of the real heat capacity with Eq. (11). The results confirm the applicability of the present method even in the case of a large apparent heat capacity.

Here, it needs to be mentioned that the calibration introduces quite a large change in its value for a large heat capacity because of the dependence of the calibration on the apparent heat capacity, as shown in Eq. (11). Therefore, the determination is less precise for a larger heat capacity as shown in Fig. 7b. In this sense, the scattering of the imaginary part shown in Fig. 6b does not mean that similar amount of error is also introduced for smaller heat capacity. Considering the error in the coefficients and obtained data, Fig. 8 shows the expected error in the real and imaginary parts of the heat capacity, which is determined from Eq. (15) for heat capacity without the imaginary part. Fig. 8 clearly suggests that the error becomes smaller for smaller heat capacity. With the present values of indium, $\widetilde{\Delta C} \sim 2000\ \mathrm{mJ\ K^{-1}}$, compared to the value of a typical polymer sample, e.g. $\widetilde{\Delta C} \leq 100\ \mathrm{mJ\ K^{-1}}$, the error must be much smaller for polymer samples.

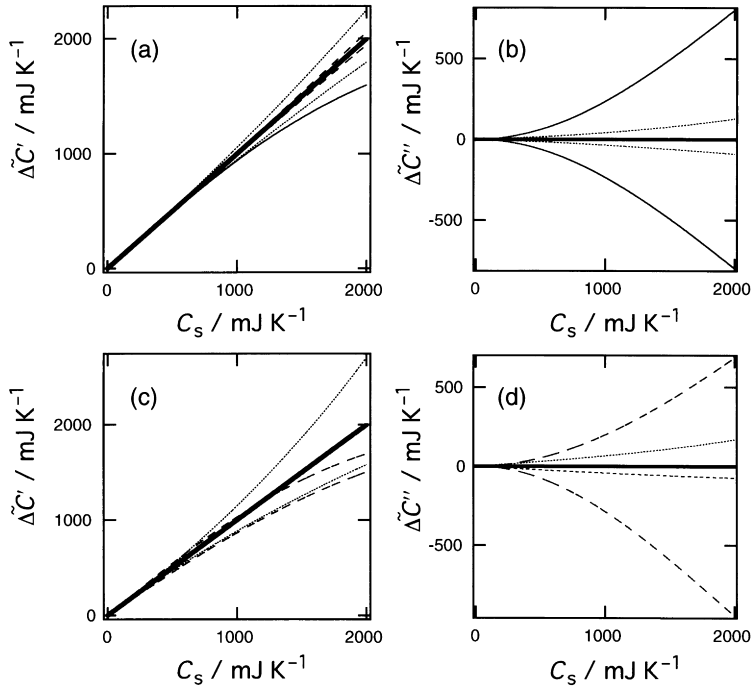

Fig. 8. Plots of the real and imaginary parts calculated for real heat capacity C_s from Eq. (15) with 10% error in τ_m (dotted lines), δ_m (broken lines) or $(1/K_1)$ (thin lines) in (a) and (b) and with ±2° or 10% error in φ (dotted lines) or C_0 (broken lines) in (c) and (d), respectively. When calculated without the errors, $\widetilde{\Delta C}' = C_s$ and $\widetilde{\Delta C}'' = 0$ (thick lines). The errors are evaluated for the modulation period of 30 s and the typical values of $\tau_m = 1.2$ s, $\delta_m = 0.26$ s and $K_1^{-1} = 0.012$ s K mJ^{-1} at 130°C with helium purge gas.

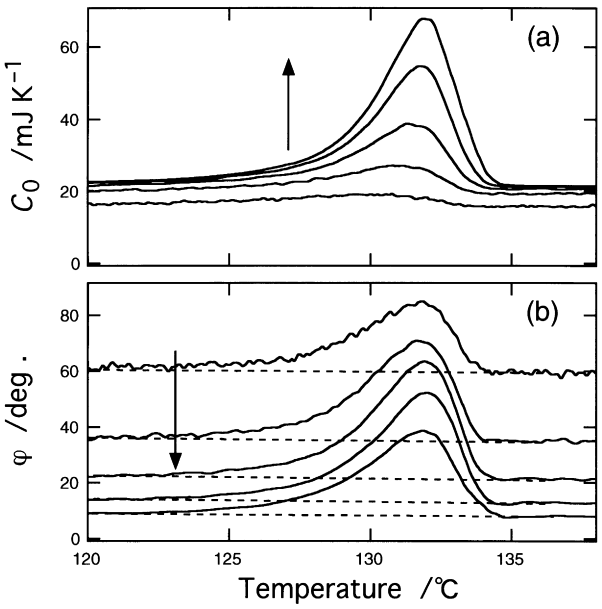

Fig. 9. Plots of the raw data of: (a) magnitude; and (b) phase angle of the apparent heat capacity in the melting region of polyethylene. The modulation periods were 10, 17, 28, 47 and 78 s. The arrows indicate the direction of longer modulation period. The purge gas was helium. The underlying heating rate was 0.8 K min^{-1} and a heating-only condition was applied. The sample mass was 1.09 mg. The broken lines in (b) represent baselines for the phase angle, assumed in the baseline-subtraction.

5. Application 2

In the following, we discuss the calibration of the complex heat capacity in the melting region of polymer crystals.

5.1. Melting of polymer crystals

Polymer crystals are the aggregates of thin lamellar crystallites. The melting points distribute over a wide temperature range (e.g. ≥20 K) due to the distributions of lamellar thickness and molecular mass. Because of the wide distribution of melting points, we expect a pseudo-steady response of the kinetics when a linear heating rate, β, is applied.

The analytical formulation [5,6] and numerical simulation [8] of the melting kinetics have suggested that the apparent heat capacity is roughly approximated by a frequency response function of Debye's type represented as,

$$\widetilde{\Delta C}\,\mathrm{e}^{-\mathrm{i}\alpha} = C_\mathrm{s} + \frac{|F_\mathrm{melt}|/\beta}{1 + \mathrm{i}\omega\tau(\beta)}, \tag{16}$$

where F_melt represents the endothermic heat flow of melting and τ is the characteristic time of melting of a crystallite. It is noted that the heating rate dependence of $\tau(\beta) \propto \beta^{-x}$ is determined by the superheating, ΔT, dependence of a melting rate coefficient of crystallites, $R(\Delta T)$, represented as $R \propto \Delta T^{x/(1-x)}$. The expression of Eq. (16) corresponds to the analytical solution for $\tau \propto \beta^0$ and β^{-1} (R independent of ΔT and proportional to $\mathrm{e}^{a\Delta T}$, respectively) but is a rough approximation for $\tau \propto \beta^{-1/2}$($R \propto \Delta T$); the analytical solution for $\tau \propto \beta^{-1/2}$ has a larger peak of the imaginary part, as seen in Fig. 15.

A frequency dispersion, roughly approximated by Eq. (16), has been reported experimentally for the melting kinetics of poly(ethylene terephthalate) [5] polyethylene [6] and nylon 6 [7] crystals. On the assumption that the re-crystallization and re-organization processes are insensitive to temperature modulation, the frequency dispersion has been attributed to the response of the melting kinetics [5–7]; the assumption is based on the fact that the response of polymer crystallization is much smaller than the response in the melting region [9–11].

In the analysis of the experimental results, such as shown in Fig. 9, a calibration has been employed without considering the change in sample heat capacity [5–7]. In this method, the calibration coefficient of the magnitude has been adjusted for the data outside the transition region. Concerned with the phase angle, a baseline such as shown in Fig. 9b has been chosen to set the phase angle to 0° outside the transition region. Therefore, this calibration method named "baseline-subtraction" corresponds to the assumption of

$$\frac{1}{K_1}\widetilde{\Delta C}\mathrm{e}^{-\mathrm{i}\alpha} = \frac{1}{K_1}C_\mathrm{s}$$

in Eq. (14) and ignores the effect of the change in the apparent heat capacity. Since the apparent heat capacity has a large peak in the melting region, as shown in Fig. 9a, the baseline-subtraction is not justified on the basis of the present calibration method. However, the discrepancy can be within an acceptable limit for sufficiently small change in $\widetilde{\Delta C}$ or large K_1 in the term of

$$\frac{1}{K_1}\widetilde{\Delta C}\mathrm{e}^{-\mathrm{i}\alpha}$$

of Eq. (14). If it is the case, the baseline-subtraction is more practical because the determination of the coefficients, τ_m, δ_m and $(1/K_1)$, required for the present calibration is quite laborious.

In the following, we apply the present calibration method and the baseline-subtraction to the melting kinetics of polymer crystals to see the applicability of the baseline-subtraction method.

5.2. Numerical calculation

Fig. 10 shows the frequency response function of Debye's type and the results of the baseline-subtraction; the raw data were calculated using Eq. (14) from the response function. The coefficients, τ_m, δ_m and $(1/K_1)$, obtained with helium and nitrogen purge gases are examined in the calculation with typical values of C_s, F_melt and τ in the melting region of polymer crystals. When we compare those results in the Cole–Cole plot of Fig. 10c, it is seen that the

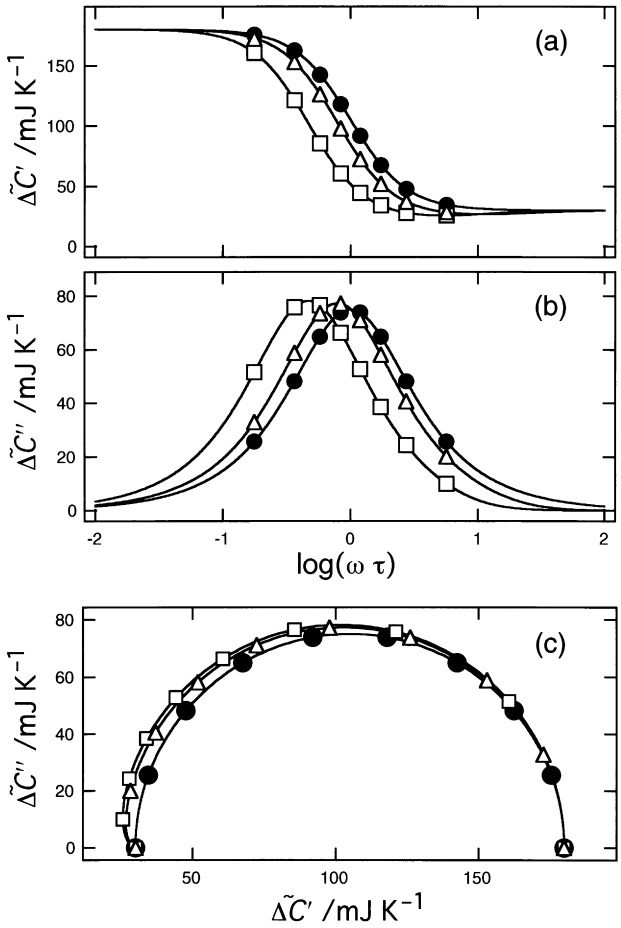

Fig. 10. Numerical calculation of the frequency response function of Debye's type (●) and the results of the baseline-subtraction (△, □) of the apparent heat capacity for the typical values of $C_s = 30$ mJ K^{-1}, $F_{melt} = 150$ mJ K^{-1}, and $\tau = 10$ s of Eq. (16) in the melting region of polymers. The symbols, △ and □, are for helium and nitrogen purge gases, respectively.

baseline-subtraction gives the correct value when extrapolated to $\omega \to 0$. The agreement is expected since the term

$$\frac{\omega}{K_1}\widetilde{\Delta C}\, e^{-i\alpha}$$

in Eq. (14) vanishes for $\omega \to 0$. Therefore, the argument [5–8] about the limiting behavior of "reversing" heat flow, $-\beta\widetilde{\Delta C}(\omega \to 0) = -\beta C_s + F_{melt}$, is valid irrespective of the choice of calibration method.

On the other hand, a larger discrepancy may be expected for higher frequency ($\omega \to \infty$) because of the term,

$$\frac{\omega}{K_1}\widetilde{\Delta C}\, e^{-i\alpha},$$

but this is not the case. For $\omega\tau \gg 1$ in Eq. (16), the change in the apparent heat capacity becomes negligible, namely

$$C_s - i\frac{|F_{melt}|/\beta}{\omega\tau} \sim C_s,$$

and hence the discrepancy also becomes negligible, as is shown in Fig. 10c. However, if one applies an extrapolation to $\omega \to \infty$ from the intermediate values, Fig. 10c also indicates that the extrapolated value can be smaller than the true value of C_s.

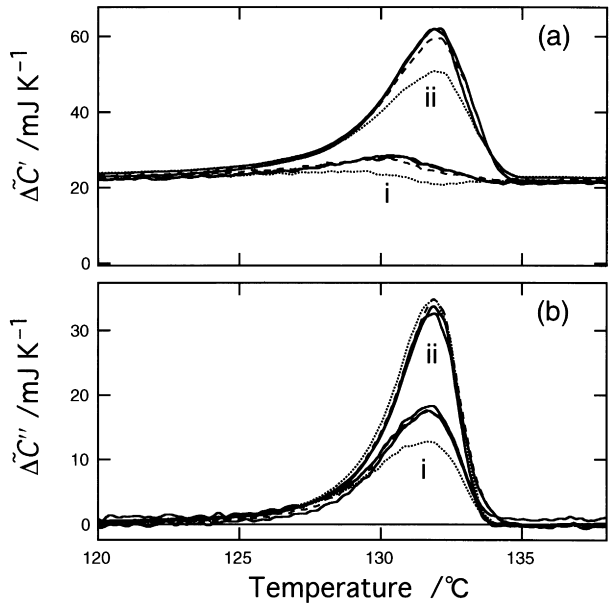

Fig. 11. Plots of the (a) real and (b) imaginary parts of the calibrated heat capacity in the melting region of polyethylene. The full lines represent the results of the present calibration with helium and nitrogen purge gases, the broken and dotted lines the results of the baseline-subtraction with helium and nitrogen purge gases, respectively. The modulation periods were: (i) 17 s; and (ii) 78 s. The underlying heating rate was 0.8 K min^{-1} and the heating only condition was applied. The sample mass was 1.09 mg.

An important discrepancy is seen in the shift of the peak frequency of the imaginary part and the corresponding shift in the real part with the baseline-subtraction. The characteristic time, τ, is evaluated from the peak frequency, ω_{peak}, with the relation, $\omega_{peak}\tau = 1$, and hence the shift to lower frequency of the peak causes the overestimation of τ.

For better thermal conductivity of the purge gas, the heat-transfer coefficient, K_1, in Eq. (14) increases, and hence the influence of sample heat capacity becomes smaller and the discrepancy between the calibration methods is expected to be smaller. With helium purge gas, it is actually seen that the baseline-subtraction reproduces the original response function better than with nitrogen purge gas.

5.3. Experimental examination

Fig. 11 shows the calibrated results of the real and imaginary parts of the apparent heat capacity in the melting region of polyethylene. While the baseline-subtraction gives different results for the purge gases of helium and nitrogen, the agreement of the present calibration for different purge gases is satisfactory. It is also seen that the baseline-subtraction with helium purge gas gives almost the same values as the results of the present calibration method. The same conclusion can be made for the frequency dependence of

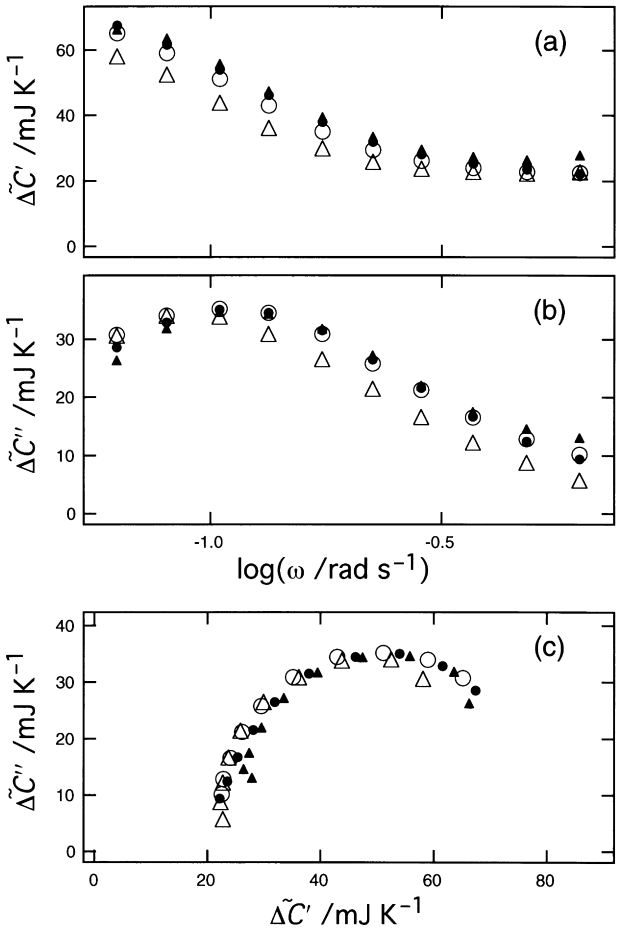

Fig. 12. Frequency dependence and (c) Cole–Cole plot of the (a) real and (b) imaginary parts of the apparent heat capacity taken at the peak temperature (132°C) in the plot such as shown in Fig. 11. The symbols, ● and ▲, represent the values calibrated by the present method with helium and nitrogen purge gases, respectively, and ○ and △ by the baseline-subtraction with helium and nitrogen purge gases, respectively. The underlying heating rate was 0.8 K min^{-1} and heating only condition was applied. The sample mass was 1.09 mg.

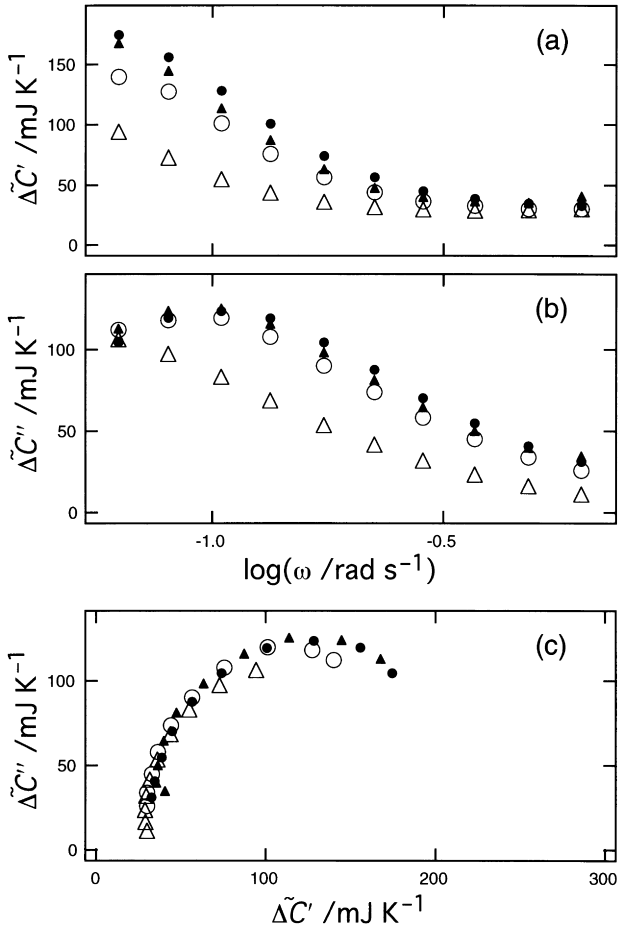

Fig. 13. Frequency dependence and (c) Cole–Cole plot of the (a) real and (b) imaginary parts of the apparent heat capacity under the same condition as in Fig. 12 except for the heavier sample mass of 4.01 mg. The symbols have the same meaning as in Fig. 12.

the peak values shown in Fig. 12. It is also seen that the essential features of the present experimental results agree with our previous results and are well reproduced by the numerical calculation in Fig. 10. In Fig. 12, although the frequency range is not wide enough to show the whole frequency dispersion, the Cole–Cole plot in Fig. 12c indicates the relation of $\widetilde{\Delta C}''_{\max}/\{\widetilde{\Delta C}'(\omega=0)-\widetilde{\Delta C}'(\omega=\infty)\} \sim 0.6$, which is in accordance with the analytical solution for $\tau \propto \beta^{-1/2}$ (ratio ~0.6) and roughly approximated by Debye's type (ratio = 0.5).

For a heavier sample shown in Fig. 13, the discrepancy between the two calibration methods becomes larger because of the term, $\widetilde{\Delta C}\,e^{-i\alpha}/K_1$, in Eq. (14), especially for the nitrogen purge gas. From the comparison of those results shown in Figs. 12 and 13 with different sample masses; it will be concluded that the baseline-subtraction with helium purge gas will be acceptable for the change in heat capacity in the examined range. With nitrogen purge gas, it is important to prepare small sample mass. A safe criterion for the applicability of the baseline-subtraction will be given by the examination with both nitrogen and helium purge gases; smaller difference between the results of the baseline-subtraction shown in Fig. 12 indicates a better calibration than in the case shown in Fig. 13.

The mass of the sample has an additional effect on the data analysis due to the thermal conductivity of the sample. To obtain a reasonable result, the temperature of the sample needs to be modulated in-phase. The sample thickness, L, must be thin enough to satisfy the condition expressed as,

$$L \ll \left(\frac{2\kappa}{\omega\rho c}\right)^{1/2}, \tag{17}$$

where ρ represents the density, c the specific heat capacity, and κ the thermal conductivity [25]. For a typical polymer (e.g. polyethylene at room temperature: $\rho \sim 10^6$ g m^{-3}, $c \sim 1.5$ J g^{-1} K^{-1} and $\kappa \sim 0.3$ W m^{-1} K^{-1}) with the modulation period of 10 s, the upper limit of the thickness, $L_{\max}$,

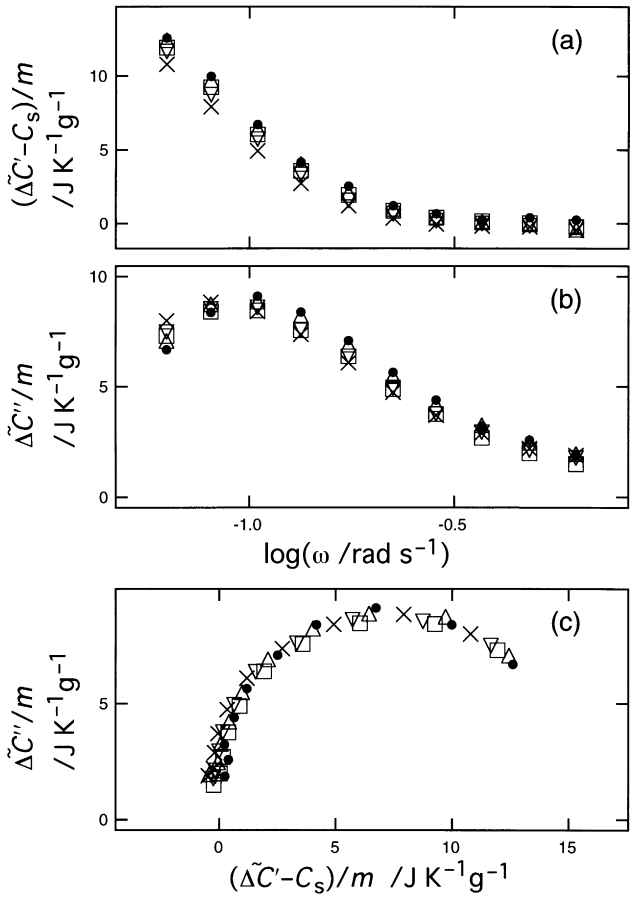

Fig. 14. Frequency dependence and (c) Cole–Cole plot of the (a) real and (b) imaginary parts of the apparent heat capacity taken at the peak temperature (222°C) in the melting region of nylon 6 crystals. The excess heat capacity was normalized by the sample mass, m. Different thicknesses/masses of the sample were examined for the symbols: 30/1.02 (●), 110/3.23 (△), 190/5.58 (□), 340/9.14 (▽) and 530 μm/13.38 mg (×). The underlying heating rate was 1.6 K min^{-1} and the heating-only condition was applied. The purge gas was helium.

will be around 500 μm, based on the estimation,

$$L_{\max} \sim 0.6 \times \left(\frac{2\kappa}{\omega\rho c}\right)^{1/2},$$

for a 99% precision of the heat capacity [25]. However, for the melting region, the heat capacity in the estimation of Eq. (17) must be the apparent heat capacity $\tilde{\Delta C}$ with the contribution of the endothermic heat flow of melting instead of the true heat capacity, and hence the upper limit of the thickness is expected to be much thinner. Fig. 14 shows the results for different sample thicknesses of nylon 6 crystals after the correction with the present calibration method. The systematic shift of the results confirms the effect of sample thickness, though the effect is not large. The evaluation of the characteristic time from the peak frequency will not be strongly influenced by the thickness in this range. The results may suggest that a sample thickness thinner than 100 μm is preferable.

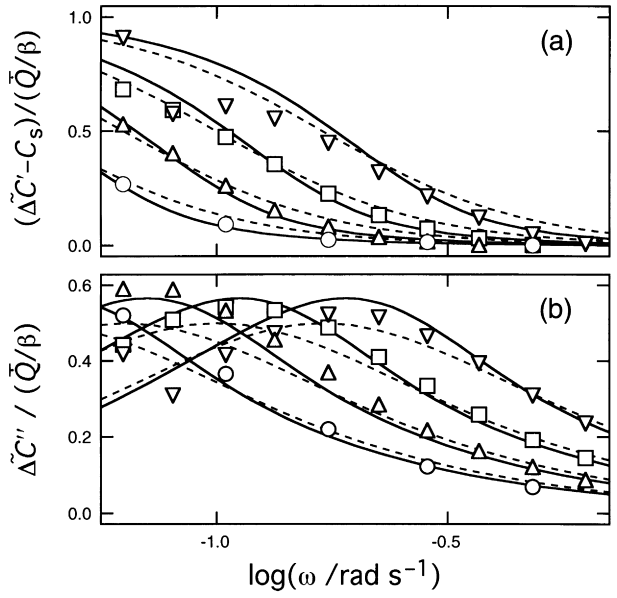

Fig. 15. Frequency and heating rate dependences of the (a) real and (b) imaginary parts of the apparent heat capacity at the peak temperature (132°C) in the melting region of polyethylene. The excess heat capacity was normalized by the endothermic heat flow of melting, $\bar{Q}$, divided by heating rate, β. The underlying heating rate was 0.2 (○), 0.4 (△), 0.8 (□) and 1.6 K min^{-1} (▽). The heating-only condition was applied. The broken lines represent the fitting by the Debye-type response function and the full lines by an analytical solution for $\tau \propto \beta^{-0.5}$ [5]. The sample mass was 1.09 mg.

In the preceding studies on the melting kinetics of polymer crystals [5–7], the authors applied the baseline-subtraction with nitrogen purge gas and hence the characteristic time, τ, may have been overestimated, as discussed above. Based on the present calibration method, we have re-examined the frequency and heating-rate dependence of the melting behavior, as shown in Fig. 15. The results confirm the frequency dependence roughly approximated by the Debye's function and the heating-rate dependence of the characteristic time, τ. Fig. 16 shows τ of the polyethylene and nylon 6 crystals plotted against heating rate; the results are similar to the previous ones, though the absolute values for polyethylene are shorter by 50% than the previous results [6]. The discrepancy is mainly due to a larger mass of the sample (4.01 mg) in the previous experiments with nitrogen as purge gas; the effect of sample mass for the baseline-subtraction is clearly seen in the comparison of Figs. 12 and 13. Since the change in the apparent heat capacity in the melting region of nylon 6 is much smaller than that of polyethylene, the results of nylon 6 show a better agreement between the present calibration and the baseline-subtraction with nitrogen purge gas.

6. Conclusion

In the present paper, we have experimentally examined the calibration of an apparent complex heat capacity in the

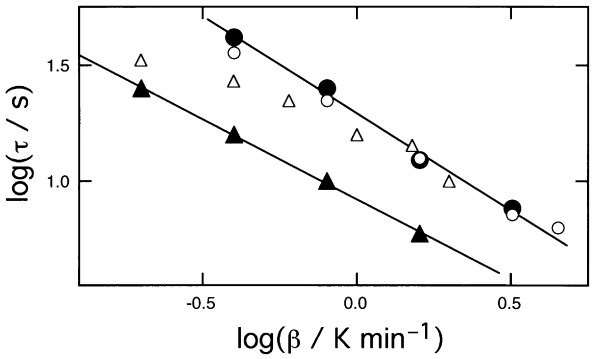

Fig. 16. Logarithmic plots of the characteristic time, τ, chosen for fitting such as shown in Fig. 15 against underlying heating rate. The symbols represent the values of nylon 6 (○, ●) and of polyethylene (△, ▲). The open symbols are the results of the previous work [1,2] obtained by the baseline-subtraction with nitrogen purge gas and the filled symbols the results of the present calibration with helium purge gas. The sample masses were 2.49 (●) and 3.50 mg (○) for nylon 6 and 1.09 (▲) and 4.01 mg (△) for polyethylene. The slopes of the straight lines are −0.84 and −0.69 for ● and ▲, respectively.

melting region of polymer crystals, based on Hatta's model considering the thermal conductivity of the DSC apparatus of heat flux type. The instrument's coefficients, τ_m, δ_m and $(1/K_1)$, are required for the calibration and have been determined experimentally by examining the dependence of the raw data of aluminum on frequency and sample heat capacity. It has been shown that the heat-transfer coefficient, K_1, between the bottom of sample pan and base plate can be controlled by a careful sample preparation. The applicability of the calibration method has been confirmed with the reversible melting and crystallization of indium, which is expected to follow the temperature modulation without delay. The raw data of the heat capacity shows a large peak of the real and imaginary parts in the transition region, while the calibrated apparent heat capacity becomes a real quantity, as expected for the fast response of transitions.

For the melting region of polymer crystals, the frequency and heating rate dependences of complex heat capacity has been reexamined with the calibration method presented here. The results confirmed the dependence roughly approximated by the frequency response function of Debye's type with the characteristic time that depends on underlying heating rate. The applicability of the baseline-subtraction to the phase angle has also been examined and justified when the sample mass is small enough. Helium purge gas provides a better thermal conductivity between the bottom of the sample pan and the base plate and hence gives a smaller coefficient to sample heat capacity in the calibration, which improves the applicability of the baseline-subtraction neglecting the change in sample heat capacity. Calibration of the baseline-subtraction is much easier than the present method that requires the determination of the instrument's coefficients with known samples. Hence, better thermal conductivity of purge gas may be preferable on this point. However, better thermal conductivity sacrifices the sensitivity to a small peak in heat flow because of heat transfer to/from the surroundings. It is therefore important to take a proper choice of purge gas for the purpose of the measurement with T-MDSC.

Acknowledgements

The authors thank Prof. Wunderlich (University of Tennessee) for valuable discussions. This work was partly supported by a Grant-in-Aid for Scientific Research from the Ministry of Education, Science and Culture of Japan and by Inoue Foundation for Science.

References

[1] Toda A, Oda T, Hikosaka M, Saruyama Y. Polymer 1997;38:231.
[2] Toda A, Oda T, Hikosaka M, Saruyama Y. Thermochim Acta 1997;293:47.
[3] Toda A, Tomita C, Hikosaka M, Saruyama Y. Polymer 1997;38:2849.
[4] Toda A, Tomita C, Hikosaka M, Saruyama Y. Polymer 1998;39:1439.
[5] Toda A, Tomita C, Hikosaka M, Saruyama Y. Polymer 1998;39:5093.
[6] Toda A, Tomita C, Hikosaka M, Saruyama Y. Thermochim Acta 1998;324:95.
[7] Toda A, Tomita C, Hikosaka M. J Therm Anal 1998;51:623.
[8] Toda T, Arita C, Tomita M. Thermochim Acta 1999;330:75.
[9] Gill PS, Sauerbrunn SR, Reading M. J Therm Anal 1993;40:931.
[10] Reading M, Elliott D, Hill VL. J Therm Anal 1993;40:949.
[11] Reading M, Luget A, Wilson R. Thermochim Acta 1994;238:295.
[12] Wunderlich B, Jin Y, Boller A. Thermochim Acta 1994;238:277.
[13] Boller A, Jin Y, Wunderlich B. J Therm Anal 1994;42:307.
[14] Hatta I. Jpn J Appl Phys 1994;33:L686.
[15] Ozawa T, Kanari K. Thermochim Acta 1996;288:39.
[16] Saruyama Y. Thermochim Acta 1996;283:157.
[17] Schawe JEK, Winter W. Thermochim Acta 1997;298:9.
[18] Weyer S, Hensel A, Schick C. Thermochim Acta 1997;305:267.
[19] Van Assche G, Van Hemelrijck A, Van Mele B. J Therm Anal 1997;49:443.
[20] Höhne GWH, Shenogina NB. Thermochim Acta 1998;310:47.
[21] Jiang Z, Imrie CT, Hutchinson JM. Thermochim Acta 1998;315:1.
[22] Hatta I, Muramatsu S. Jpn J Appl Phys 1996;35:L858.
[23] Ishikiriyama K, Boller A, Wunderlich B. J Therm Anal 1997;50:547.
[24] Chen W, Dadmun M, Zhang G, Boller A, Wunderlich B. Thermochim Acta 1998;324:87.
[25] Hatta I, Minakov AA. Thermochim Acta 1999;330:39.